PHYSICAL REVIEW B VOLUME 35, NUMBER 7 1 MARCH 1987

Hyperfine fields of 3d and 4d impurities in nickel

S. Blügel, H. Akai,* R. Zeller, and P. H. Dederichs
Institut für Festkörperforschung der Kernforschungsanlage, Jülich, D5170 Jülich, Federal Republic of Germany
(Received 24 September 1986)

We present detailed calculations of the electronic structure and the hyperfine fields of $3d$ and $4d$ impurities in nickel. The calculations are based on the local-density approximation of density-functional theory and the Korringa-Kohn-Rostoker Green's-function method for impurity calculations. We self-consistently calculate the local moments and hyperfine fields of the impurities and their nearest neighbors. We derive new formulas for the proper relativistic generalizations of the contact, orbital, and dipolar contributions to the hyperfine field and explicitly calculate relativistic corrections to the contact interaction which are important for $4d$ impurities. The hyperfine fields can be split up into local and transferred contributions which are directly related to the local moments and to the moments of the neighboring atoms. The calculated hyperfine fields are in reasonable agreement with the experimental data.

I. INTRODUCTION

Hyperfine fields provide unique microscopic information about dilute ferromagnetic alloys. The dominant contribution to the hyperfine field results from the Fermi contact interaction and is given by the magnetization density at the nucleus. There exists a huge amount of experimental information about hyperfine fields of impurities in Fe, Co, Ni, and Gd which can be found in two recent data collections by Rao[1] and Krane.[2] The theoretical understanding of hyperfine fields in alloys was rather limited up to recently. While the earlier model calculations of Daniel and Friedel[3] could explain the negative hyperfine field of the early *sp* impurities, the work of Katayama-Yoshida, Terakura, and Kanamori[4–6] has lead to an understanding of the systematic trends of the hyperfine fields of *sp* impurities. These authors pointed out that the hybridization of the impurity *s* with the host *d* orbitals leads to bonding and antibonding peaks for both spin directions and that the intensities as well as the positions of these peaks directly determine the hyperfine fields.

While *sp* impurities are nonmagnetic, $3d$ and $4d$ impurities have a local moment in ferromagnets which complicates the situation considerably. The contribution to the hyperfine field which is transferred by hybridization from the polarized neighboring *d* electrons ("transferred" hyperfine field) is supplemented by a "local" contribution due to the polarization of the local core and valence *s* electrons by the local *d* shell. This requires a self-consistent treatment of the electronic structure problem. Moreover an "all electron" calculation has to be performed, since core relaxations have to be taken into account due to the importance of the core polarization. Band-structure calculations by Janak[7] for the pure metals Fe, Co, and Ni were based on the local-density approximation and led to considerable success, i.e., quite accurate hyperfine field values for Ni and Co, while the value for Fe was off by 25%. This is surprising in view of the work of Wilk and Vosko[8] who concluded on the basis of atomic calculations that it would not be possible to calculate the hyperfine fields of local moment systems by the local-density approximation and that a more serious treatment of the intra-atomic exchange is required.

Recently Akai, Akai, and Kanamori[9,10] have performed self-consistent calculations for $3d$ and $4d$ impurities in Fe. As in the work of Katayama-Yoshida *et al.*[4–6] in these calculations the Korringa-Kohn-Rostoker (KKR) Green's function method for point-defect calculations is applied,[11] however contrary to the previous work the Fe potential is calculated self-consistently. Similar, but slightly less sophisticated, calculations have also been performed by Leonard and Stefanou.[12]

Partly in parallel to this effort first self-consistent calculations for $3d$ and $4d$ impurities in Ni were performed by Zeller.[13] These calculations have been extended so that also potential perturbations on the neighboring sites are included. A detailed account of the calculations, especially for the impurity moments and the perturbed moments on the neighboring sites will be given in a separate publication.[14] In parallel with the work of Akai *et al.* for Fe, calculations of the hyperfine fields for $3d$ and $4d$ impurities in Ni were performed by Blügel.[15] The present paper is the result of a combined effort of both groups and represents a considerable extension of the work of Akai *et al.* Since both the impurity potential as well as the potential of the neighboring atoms are determined self-consistently we can calculate the hyperfine fields of both the impurity and the nearest neighbors. Moreover we estimate also relativistic corrections to the hyperfine fields in the scalar relativistic approximation, in which the orbital contribution is neglected.

The organization of the paper is as follows. Section II deals with the description of the theoretical method, in particular the scalar relativistic extension of the KKR Green's function method. In Sec. III we derive, starting from the work of Breit,[16] the proper relativistic expressions for the contact, orbital, and dipolar contributions to the hyperfine field. In Sec. IV we present detailed calculations for the local moments of the impurities and their nearest neighbors. Especially we discuss the numerical re-

liability of the calculations and the sensitivity of the results with respect to approximations of the exchange correlation energy. Finally, Sec. V gives the results for the calculated hyperfine fields of the impurities and a comparison with the experimental data. Two questions are considered in detail. Can the local density approximation provide us with reliable values for the hyperfine fields? In view of the strongly inhomogeneous core polarization this is not clear at all. Second, what information can measured hyperfine fields give us about the electronic structure and especially the local moments? Section V deals also with the change of the hyperfine fields of the nearest-neighbor atoms.

A preliminary account of this work has been given in a conference paper.[17] Preliminary results for impurities in Fe are given in Ref. 18.

II. THEORETICAL METHOD

Our calculations are based on density-functional theory in the local-spin-density approximation. Several different forms for the local exchange correlation energy are used: the form of von Barth and Hedin,[19] the version used by Moruzzi, Janak, and Williams,[20] and the recent expression of Vosko, Wilk, and Nusair,[21] which has been fitted to the results of many-body calculations for the homogeneous electron gas by Monte Carlo methods.[22]

For the impurity calculations we employ the KKR Green's function method, which is based on the KKR band structure method for ideal crystals. We generate the band structure of pure Ni from the self-consistent potentials given by Moruzzi *et al.*[20] and construct the one-electron Green's function $\mathring{G}(\mathbf{r},\mathbf{r}';E)$ of ideal Ni from the calculated energy eigenvalues and wave functions. For details about this procedure we refer to Refs. 11 and 23. The Dyson equation for the Green's function $G(\mathbf{r},\mathbf{r}';E)$ of the defect crystal is given by

$$G(\mathbf{r},\mathbf{r}';E)=\mathring{G}(\mathbf{r},\mathbf{r}';E)+\int \mathring{G}(\mathbf{r},\mathbf{r}'';E)\Delta V(\mathbf{r}'')G(\mathbf{r}'',\mathbf{r}';E)d\mathbf{r}'' , \tag{1}$$

where $\Delta V(\mathbf{r})=V(\mathbf{r})-\mathring{V}(\mathbf{r})$ is the potential perturbation being localized near the defect. We allow perturbed potentials for the impurity and for the 12 nearest neighbors.

The perturbed potentials are either of muffin-tin form, as the ones in the ideal crystal, or of Wigner-Seitz form, i.e., spherically symmetric inside the Wigner-Seitz sphere. In the latter case the potentials are partially overlapping and KKR theory is not strictly valid for such potentials. However, it is thought that the errors involved are smaller than the improvements gained by the fact that the potentials are better filling up the space. This is an important argument for impurity calculations, since the muffin-tin zero potential is determined by the host and cannot be changed near the impurity. Thus we consider a cluster of 13 Wigner-Seitz potentials being embedded in an otherwise ideal crystal of muffin-tin potentials. Our calculations show, that both for the local moments and for the hyperfine fields the differences between the muffin-tin and Wigner-Seitz results are very small and insignificant. This is not necessarily also true for other physical properties. For instance Gunnarsson *et al.*[24] find that atomic sphere potentials yield important improvements in total-energy calculations. Similarly we find important differences in isomer shift calculations.[25] Since the differences between both calculations are so small, the results given in the following sections will only refer to Wigner-Seitz potentials. The charge density inside the cluster is completely redetermined in each iteration and the ideal crystal potential is only used to describe the embedding of this cluster into the ideal crystal. Compared to our previous calculations[23] where only the charge perturbations $\Delta\rho$ and potential perturbations ΔV are recalculated inside the cluster, this has the advantage that inside the cluster different exchange correlation potentials can be used as well as relativistic corrections can be applied without changing the host Green's functions (see below).

In the KKR Green's function method one works with a double expansion of the Green's function $G(\mathbf{r}+\mathbf{R}^n, \mathbf{r}'+\mathbf{R}^{n'};E)$ into radial eigenfunctions of the local muffin-tin potentials. Of central importance are the expansion coefficients $G_{LL'}^{nn'}(E)$, the so-called structural Green's functions. They are related to the corresponding expansion coefficients $\mathring{G}_{LL'}^{nn'}(E)$ by a Dyson equation. For details about the method and the calculational procedure we refer to Ref. 23. Here we will shortly discuss a scalar relativistic extension of the Green's function method.

One possible way of solving the Dirac equation is the elimination method.[26] By decomposing the four-spinor ψ_α ($\alpha=1,2,3,4$) into a large component Φ_1 and a small component Φ_2 one obtains the coupled equations

$$\begin{aligned}&[mc^2-E+V(\mathbf{r})]\Phi_1+c\boldsymbol{\sigma}\cdot\mathbf{p}\Phi_2=0 ,\\ &c\boldsymbol{\sigma}\cdot\mathbf{p}\Phi_1-[mc^2+E-V(\mathbf{r})]\Phi_2=0 .\end{aligned} \tag{2}$$

By inserting the preceding equation

$$\Phi_2=\frac{1}{2mc^2+\epsilon-V(\mathbf{r})}c\boldsymbol{\sigma}\cdot\mathbf{p}\Phi_1,\quad E=mc^2+\epsilon \tag{3}$$

into the first one, we obtain an equation for the large component alone. Using the operator identity[27]

$$\boldsymbol{\sigma}\cdot\mathbf{A}\boldsymbol{\sigma}\cdot\mathbf{B}=\mathbf{A}\cdot\mathbf{B}+i\boldsymbol{\sigma}\cdot(\mathbf{A}\times\mathbf{B}) , \tag{4}$$

this can be written as a Schrödinger-type equation with an energy-dependent potential

$$\left[\frac{\mathbf{p}^2}{2m}+\tilde{V}(\mathbf{r},\epsilon)-\epsilon\right]\Phi_1=0 \tag{5}$$

with

$$\tilde{V}(\mathbf{r},\epsilon)=V(\mathbf{r})+\frac{1}{2m}\boldsymbol{\sigma}\cdot\mathbf{p}\left[\frac{1}{1+\frac{\epsilon-V(\mathbf{r})}{2mc^2}}-1\right]\boldsymbol{\sigma}\cdot\mathbf{p} .$$

Defining the relativistic mass $M(\mathbf{r})=m+[\epsilon-V(\mathbf{r})]/2c^2$ the potential can also be written as

$$\tilde{V}(\mathbf{r},\epsilon)=V(\mathbf{r})+\left[\frac{1}{2M(\mathbf{r})}-\frac{1}{2m}\right]p^2-\frac{\hbar^2}{4M^2(\mathbf{r})c^2}\frac{\partial V}{\partial \mathbf{r}}\cdot\partial_{\mathbf{r}}+\frac{1}{4M^2(\mathbf{r})c^2}\sigma\cdot\left[\frac{\partial V}{\partial \mathbf{r}}\times\mathbf{p}\right]. \tag{6}$$

The last term is the spin-orbit coupling term. For the charge density $n(\mathbf{r})$ one obtains

$$n(\mathbf{r})=\sum_{s=1}^{2}[\,|\Phi_{1s}(\mathbf{r})|^2+|\Phi_{2s}(\mathbf{r})|^2]$$

$$=\sum_{s=1}^{2}\left[|\Phi_{1s}(\mathbf{r})|^2+\frac{\hbar^2}{4M^2(\mathbf{r})c^2}\left|\frac{\partial\Phi_{1s}}{\partial\mathbf{r}}\right|^2\right]+\sum_{s,s'=1}^{2}\left[\frac{\hbar^2}{4M^2(\mathbf{r})c^2}\right]\sigma_{ss'}\cdot\left[\frac{\partial\Phi^*_{1s}(\mathbf{r})}{\partial\mathbf{r}}\times\frac{\partial\Phi_{1s'}(\mathbf{r})}{\partial\mathbf{r}}\right]. \tag{7}$$

Again the last term represents a spin-orbit—type contribution to the charge density.

In the scalar relativistic approximation[28,29] one completely neglects spin-orbit couplings. This amounts to replacing the potential $\tilde{V}(\mathbf{r},\epsilon)$ in Eq. (5) by

$$\tilde{V}(\mathbf{r},\epsilon)=V(\mathbf{r})+\frac{1}{2m}\mathbf{p}\left[\frac{1}{1+\dfrac{\epsilon-V(\mathbf{r})}{2mc^2}}-1\right]\mathbf{p} \tag{8}$$

and the charge density in Eq. (7) by

$$n(\mathbf{r})=\sum_{s=1}\left[|\Phi_{1s}(\mathbf{r})|^2+\frac{\hbar^2}{4M^2(\mathbf{r})c^2}\left|\frac{\partial\Phi_{1s}}{\partial\mathbf{r}}\right|^2\right]. \tag{9}$$

The main advantage of the scalar relativistic approximation is that spin remains a good quantum number, and magnetic problems can be treated with the same ease as in the nonrelativistic theory. For a central symmetric potential also angular momentum is a good quantum number.[27]

The above discussion can be easily extended to the Dirac Green's function, representing a 4×4 spinor matrix. By decomposition into 2×2 submatrices we obtain in matrix form

$$\begin{bmatrix}V(\mathbf{r})-\epsilon & c\sigma\cdot\mathbf{p}\\ c\sigma\cdot\mathbf{p} & -2mc^2-\epsilon+V(\mathbf{r})\end{bmatrix}\begin{bmatrix}G_{11} & G_{12}\\ G_{21} & G_{22}\end{bmatrix}=-\begin{bmatrix}1 & 0\\ 0 & 1\end{bmatrix}. \tag{10}$$

By elimination the submatrices G_{12}, G_{21}, and G_{22} can be expressed in terms of G_{11}:

$$G_{21}=\frac{1}{2mc^2+\epsilon-V}c\sigma\cdot\mathbf{p}G_{11} \tag{11}$$

A similar equation is obtained for G_{12} if one writes Eq. (10) in the inverted form $G(H-\epsilon)=-1$:

$$G_{12}=G_{11}c\sigma\cdot\mathbf{p}\frac{1}{2mc^2+\epsilon-V}. \tag{12}$$

Inserting this expression for G_{12} into (10) one obtains for G_{22}

$$G_{22}=\frac{1}{2mc^2+\epsilon-V}+\frac{1}{2mc^2+\epsilon-V}c\sigma\cdot\mathbf{p}G_{11}c\sigma\cdot\mathbf{p}\frac{1}{2mc^2+\epsilon-V}. \tag{13}$$

G_{11} is determined by the equation

$$\left[\frac{p^2}{2m}+\tilde{V}(\mathbf{r},\epsilon)-\epsilon\right]G_{11}(\mathbf{r},\mathbf{r}';\epsilon)=-\delta(\mathbf{r}-\mathbf{r}'). \tag{14}$$

The charge density is obtained by summing $\mathrm{Im}G(\epsilon)$ over all occupied states:

$$n(\mathbf{r})=-\frac{1}{\pi}\int^{\epsilon_F}d\epsilon\,\mathrm{Im}\sum_{s=1}^{2}[G^{ss}_{11}(\mathbf{r},\mathbf{r};\epsilon)+G^{ss}_{22}(\mathbf{r},\mathbf{r};\epsilon)]. \tag{15}$$

In the scalar relativistic approximation we neglect the spin-orbit term in the potential, i.e., we replace $\tilde{V}(\mathbf{r},\epsilon)$ by Eq. (8). Furthermore, also for the charge density we neglect the spin-orbit contribution, so that

$$n(\mathbf{r})=-\frac{1}{\pi}\int^{\epsilon_F}d\epsilon\,\mathrm{Im}\sum_{s=1}^{2}\left[G^{ss}_{11}(\mathbf{r},\mathbf{r};\epsilon)+\frac{\hbar^2}{4M^2(\mathbf{r})c^2}\partial_{\mathbf{r}}\cdot\partial_{\mathbf{r}'}G^{ss}_{11}(\mathbf{r},\mathbf{r}';\epsilon)\,|_{\mathbf{r}=\mathbf{r}'}\right]. \tag{16}$$

III. RELATIVISTIC CORRECTIONS FOR THE HYPERFINE FIELD

The most important contribution to the hyperfine field is the Fermi contact interaction.[30] In this approximation the hyperfine field is given by the spin density $m(0)$ at the nuclear position

$$H_{\rm hf}=\frac{8\pi}{3}\mu_B m(0)\ ,$$

with (17)

$$m(0)=\int^{\epsilon_F} d\epsilon[n_+(0,\epsilon)-n_-(0,\epsilon)]\ .$$

Here $n_\pm(0,\epsilon)$ are the local densities of states for spin-up and -down electrons at the nuclear position. Shortly after Fermi's article, Breit[16] derived the correct relativistic expression for the hyperfine interaction showing that relativistic corrections are already important for nuclei with moderately large nuclear charges. This is essentially due to the fact that the hyperfine field is determined from the behavior of the wave functions close to the nucleus where relativistic effects are most important.

In many applications relativistic corrections to the hyperfine field are calculated by employing the contact interaction formula, but using semirelativistic wave functions averaged out over the size of the atomic nucleus.[31,32] Pyykkö, Pajanne, and Inokuti[33] and more recently Asada and Terakura[34] have shown that this leads to a serious overestimation of the relativistic effects. Due to the importance of this problem we will rederive here the correct relativistic expression for the hyperfine field due to Breit.[16] Moreover we will show that this expression can be uniquely split up into three contributions, which are relativistic generalizations of the orbital, dipolar, and contact contributions to the hyperfine field. The new formula for the contact interaction shows that in the relativistic case the spin density $m(0)$ at the nucleus has to be averaged over a small region near the nucleus whose diameter is the Thomson radius $r_T=Ze^2/mc^2$.

For the hyperfine interaction we consider the effect of the vector potential $\mathbf{A}$ produced by the nuclear moment $\mathbf{M}$,

$$\mathbf{A}(\mathbf{r})=\mathbf{M}\times\mathbf{r}/r^3=\partial_{\mathbf{r}}\times\left[\frac{\mathbf{M}}{r}\right] \tag{18}$$

on the electronic motion. We restrict ourselves to a single electron since the generalization to many electrons is straightforward. In first-order perturbation theory the change ΔE of the energy due to the vector potential $\mathbf{A}$ is given by

$$\Delta E=-e\langle\mathring{\psi}\,|\,\boldsymbol{\alpha}\cdot\mathbf{A}(\mathbf{r})\,|\,\mathring{\psi}\rangle\ , \tag{19}$$

where $\mathring{\psi}$ is an eigenspinor of the unperturbed Dirac Hamiltonian and $\boldsymbol{\alpha}=(\alpha_1,\alpha_2,\alpha_3)$ are the first three Dirac matrices. By decomposing the four-spinor $\mathring{\psi}$ into its large component Φ_1 and small component Φ_2, one obtains

$$\Delta E=-e(\langle\Phi_1\,|\,\boldsymbol{\sigma}\cdot\mathbf{A}\,|\,\Phi_2\rangle+\langle\Phi_2\,|\,\boldsymbol{\sigma}\cdot\mathbf{A}\,|\,\Phi_1\rangle)\ , \tag{20}$$

where $\boldsymbol{\sigma}=(\sigma_1,\sigma_2,\sigma_3)$ are the Pauli matrices. Using Eq. (3), the small component wave function Φ_2 can be expressed by the large component Φ_1. Introducing $S(\mathbf{r})$ as the reciprocal of the relativistic mass enhancement

$$S(\mathbf{r})=\frac{m}{M(\mathbf{r})}=\left[1+\frac{\epsilon-V(\mathbf{r})}{2mc^2}\right]^{-1}\ , \tag{21}$$

the energy change ΔE can be written as

$$\Delta E=-\frac{e}{2mc}\langle\Phi_1\,|\,\{\boldsymbol{\sigma}\cdot\mathbf{A}(\mathbf{r})S(\mathbf{r})\boldsymbol{\sigma}\cdot\mathbf{p}+\boldsymbol{\sigma}\cdot\mathbf{p}\boldsymbol{\sigma}\cdot\mathbf{A}(\mathbf{r})S(\mathbf{r})\}\,|\,\Phi_1\rangle\ . \tag{22}$$

Using the operator identity (4) for the Pauli matrices, we obtain for the bracketed operator

$$\{\boldsymbol{\sigma}\cdots\boldsymbol{\sigma}\cdots\}=2S(\mathbf{r})\mathbf{A}\cdot\mathbf{p}+\frac{\hbar}{i}\frac{\partial\mathbf{A}}{\partial\mathbf{r}}S(\mathbf{r})+\frac{\hbar}{i}\mathbf{A}\frac{\partial S}{\partial\mathbf{r}}+S(\mathbf{r})\hbar\boldsymbol{\sigma}(\partial_{\mathbf{r}}\times\mathbf{A})+\hbar\boldsymbol{\sigma}\left[\frac{\partial S}{\partial\mathbf{r}}\times\mathbf{A}\right]\ . \tag{23}$$

Due to Eq. (18), $\partial\mathbf{A}/\partial\mathbf{r}$ vanishes. For spherical potentials also $\mathbf{A}(\partial S/\partial\mathbf{r})$ vanishes. The $\boldsymbol{\sigma}$-independent term $2S\mathbf{A}\cdot\mathbf{p}$ gives rise to an orbital contribution to ΔE. Introducing the angular momentum operator $\mathbf{L}=\mathbf{r}\times\mathbf{p}$ this contribution can be written as

$$\Delta E_{\rm orbital}=-\frac{e}{mc}\mathbf{M}\left\langle\Phi_1\left|\frac{S(r)}{r^3}\mathbf{L}\right|\Phi_1\right\rangle\ . \tag{24}$$

The standard nonrelativistic orbital contribution is obtained by setting $S\equiv1$ and by identifying the large component Φ_1 with the Schrödinger wave function $\Phi_{\rm Sch}$.

The remaining spin contributions to ΔE can be evaluated by realizing that

$$\mathbf{H}(\mathbf{r})=\partial_{\mathbf{r}}\times\mathbf{A}=\partial_{\mathbf{r}}\times\left[\partial_{\mathbf{r}}\times\left[\frac{\mathbf{M}}{r}\right]\right]=\frac{8\pi}{3}\mathbf{M}\delta(\mathbf{r})-\frac{1}{r^3}[\mathbf{M}-3\hat{\mathbf{r}}(\hat{\mathbf{r}}\cdot\mathbf{M})],\quad\hat{\mathbf{r}}=\mathbf{r}/r \tag{25}$$

is the magnetic field due to the nuclear moment. The last term in (25) gives rise to the dipolar contribution

$$\Delta E_{\rm dipolar}=\left\langle\Phi_1\left|\frac{S(r)}{r^3}[\boldsymbol{\mu}\cdot\mathbf{M}-3(\boldsymbol{\mu}\cdot\hat{\mathbf{r}})(\mathbf{M}\cdot\hat{\mathbf{r}})]\right|\Phi_1\right\rangle\ , \tag{26}$$

where $\boldsymbol{\mu}=e\hbar/2mc\boldsymbol{\sigma}=\mu_B\boldsymbol{\sigma}$ is the magnetic moment operator of the electron. Again the standard nonrelativistic results follow by setting $S=1$ and by replacing Φ_1 by the Schrödinger wave function.

The two remaining terms, i.e., the $\delta(\mathbf{r})$ term from Eq. (25) and the last term from Eq. (23), give rise to the contact interaction.

$$\Delta E_{\rm contact}=-\frac{8\pi}{3}\mu_B\langle\Phi_1\,|\,S(r)\mathbf{M}\cdot\boldsymbol{\sigma}\delta(\mathbf{r})\,|\,\Phi_1\rangle-\mu_B\left\langle\Phi_1\left|\frac{1}{r^2}\frac{\partial S}{\partial r}[\mathbf{M}\cdot\boldsymbol{\sigma}-(\mathbf{M}\cdot\hat{\mathbf{r}})(\boldsymbol{\sigma}\cdot\hat{\mathbf{r}})]\right|\Phi_1\right\rangle\ . \tag{27}$$

In deriving the preceding expression we have used the ro-

tational invariance of the potential $V(r)$.

In the nonrelativistic limit we have $S\equiv 1$ and $\partial S/\partial r=0$. Therefore the second term vanishes and the first term yields the Fermi contact interaction

$$\Delta E_F=-\frac{8\pi}{3}\mu_B\mathbf{M}\cdot\mathbf{m}_{\mathrm{Sch}}(0)\ ,$$

with (28)

$$\mathbf{m}_{\mathrm{Sch}}(0)=\langle\Phi_{\mathrm{Sch}}\,|\,\sigma\delta(\mathbf{r})\,|\,\Phi_{\mathrm{Sch}}\rangle\ ,$$

where $\mathbf{m}_{\mathrm{Sch}}(0)$ is the Schrödinger spin density at the nucleus. Contrary to this in the relativistic case the first term vanishes, as can be seen as follows. For small distances, the relativistic $s_{1/2}$ and $p_{1/2}$ wave functions diverge[27] as

$$\Phi(r)\sim r^{\lambda-1},\ \text{with}\ \lambda=(1-\alpha^2Z^2)^{1/2} \tag{29}$$

where Z is the nuclear charge and $\alpha=\frac{1}{137}$ is the fine structure constant. Since $S(r)\sim(2mc^2/Ze^2)r$ for small $\mathbf{r}$, the product $|\Phi(r)|^2S(r)\sim r^{2\lambda-1}$ and vanishes for $r\to 0$, provided $Z<118$. Therefore the δ function gives no contribution and the second term in Eq. (27) is the relativistic analogue to the contact interaction. It has indeed very similar properties. For a pure Coulomb potential $V(r)=-Ze^2/r$ the derivative $\partial S/\partial r$ simulates a δ function:

$$\delta_T(\mathbf{r})=\frac{1}{4\pi r^2}\frac{\partial S}{\partial r}=\frac{1}{4\pi r^2}\frac{r_T/2}{\left[\left(1+\frac{\epsilon}{2mc^2}\right)r+r_T/2\right]^2}\ , \tag{30}$$

with

$$r_T=\frac{Ze^2}{mc^2}\ .$$

The only important contributions to the integral in Eq. (27) are obtained from r values of the order of or smaller than the Thomas radius r_T. Therefore $\delta_T(r)$ effectively represents a smeared-out δ function, since the integral

$$\int d\mathbf{r}\delta_T(r)=\frac{1}{1+\frac{\epsilon}{2mc^2}}\approx 1\ . \tag{31}$$

Since $\partial S/\partial r$ gives only important contributions for small distances, the largest contributions to the contact interaction arise from s-wave functions, for which $(\mathbf{M}\cdot\hat{\mathbf{r}})(\sigma\cdot\hat{\mathbf{r}})$ can be replaced by $\frac{1}{3}\mathbf{M}\cdot\sigma$. Taking everything together the contact interaction for s electrons is given by

$$\Delta E_{\mathrm{contact}}\cong-\frac{8\pi}{3}\mu_B\langle\Phi_1\,|\,\delta_T(\mathbf{r})\mathbf{M}\cdot\sigma\,|\,\Phi_1\rangle$$
$$=-\frac{8\pi}{3}\mu_B\mathbf{M}\mathbf{m}_{\mathrm{av}}$$

with

$$\mathbf{m}_{\mathrm{av}}=\int d\mathbf{r}'\delta_T(\mathbf{r}')\mathbf{m}(\mathbf{r}') \tag{32}$$

and

$$\mathbf{m}(\mathbf{r}')=\langle\Phi_1\,|\,\sigma\cdot\delta(\mathbf{r}-\mathbf{r}')\,|\,\Phi_1\rangle\ .$$

Thus in the relativistic case the spin density at the nuclear position has to be replaced by the average of the spin density over a region near the nucleus whose diameter is the Thomson radius r_T. Since the Thomson radius is always much larger than the nuclear radius r_n, i.e., for $Z=28$ (Ni), we have $r_T/2r_n\approx 8.5$ whereas for $Z=46$ (Pd), $r_T/2r_0\approx 11.4$, it is clear that the finite size of the nucleus is not of importance for the hyperfine field.

The continuous transition of the relativistic results with the averaged moment m_{av} to its nonrelativistic value $m_{\mathrm{Sch}}(0)$ can be understood as follows. The relativistic charge and spin densities diverge near the origin, i.e.,

$$m(r)\sim r^{2\lambda-2}\approx\frac{1}{r^{\alpha^2Z^2}},\ \text{for}\ r\ll r_T\ . \tag{33}$$

Therefore we average Eq. (33) over this divergence region so that m_{av} is always larger than the nonrelativistic value $m_{\mathrm{Sch}}(0)$. The relativistic enhancement $m_{\mathrm{av}}/m_{\mathrm{Sch}}(0)$ approaches one for small charges Z and slowly increases with increasing Z. For hydrogenic wave functions Breit[16] and Pyykkö *et al.*[33] have calculated the relativistic enhancement in the atomic case. For s-wave functions they obtain

$$\frac{m_{\mathrm{av}}}{m_{\mathrm{Sch}}(0)}\equiv B(n,Z)=\frac{n^3(2\lambda+2n-2+A^{1/3})}{\lambda(4\lambda^2-1)A^2}$$

with (34)

$$A=2(n-1)\lambda+n^2-2n+2$$
$$\approx 1+\left[\frac{11}{6}+\frac{3}{2}\frac{1}{n}-\frac{11}{6}\frac{1}{n^2}\right](Z\alpha)^2+O((Z\alpha)^4)\ .$$

For $Z=28$ (Ni), the enhancement is 9.4%, whereas for $Z=46$ (Pd), it is 28% and for $Z=78$ (Pt) it is 230% (always for the valence s electrons).

It is quite interesting to compare the relativistic enhancement of the hyperfine fields with the corresponding enhancement of the isomer shifts. The isomer shifts are determined by a certain average of the charge density over the nuclear volume.[35] In Schrödinger theory the s charge density is practically constant within the nucleus so that the finite size is unimportant. In Dirac theory the charge density at the nuclear volume is decisive and leads to an important enhancement of the isomer shifts. Since the nuclear radius is much smaller than the Thomson radius, this enhancement is appreciably larger than the one for the hyperfine fields. Shirley[36] gives a tabulation of this isomer shift enhancement factor $S(Z)$ for atoms. For $Z=28$ (Ni), $Z=46$ (Pd), and $Z=78$ (Pt), he obtains $S(Z)=1.37$, 2.18, and 8.10, respectively. Essentially the same enhancement factor is also obtained for the hyperfine field if erroneously the Fermi contact formula is used together with relativistic enhanced wave-functions averaged over the nuclear volume.[31,32] In some cases this unjustified procedure yields even a better agreement with the experimental data. For example, for pure Fe we calculate a nonrelativistic hyperfine field of -267 kG which is in reasonable agreement with Janak's value of -260 kG, but still far off the experimental value of -339 kG. A proper relativistic treatment yields -288 kG, still appreciably

lower than the experiment. However with an enhancement factor of 1.32 as appropriate for the isomer shift of Fe one obtains a value of $-267\times1.32=352$ kG in apparently good agreement with the experiment.

The preceding discussion is generalized to the case of many electrons by summing over all occupied states with energies ϵ smaller than the Fermi energy ϵ_F. In the semirelativistic approximation the large and small component wave functions Φ_1 and Φ_2 for s states are given by

$$\Phi_1=R_0^{\pm}(r)\frac{1}{\sqrt{4\pi}}|\chi^{\pm}\rangle ,$$

$$\Phi_2=-i\sigma\cdot\hat{\mathbf{r}}\rho_0^{\pm}(r)\frac{1}{\sqrt{4\pi}}|\chi^{\pm}\rangle , \tag{35}$$

with

$$\rho_0^{\pm}(r)=\frac{\hbar}{2mc}S_1(r)\partial_r R_0^{\pm}(r) ,$$

where $|\chi^{\pm}\rangle$ denotes the spin-up and -down states and $R_0^{\pm}(r)$ radial s-wave functions (for valence states being normalized in the Wigner-Seitz sphere). After some simple algebra the energy change ΔE follows as

$$\Delta E=-\frac{8\pi}{3}\mu_B M\int^{\epsilon_F}d\epsilon[F_0^{+}(\epsilon)n_0^{+}(\epsilon)-F_0^{-}(\epsilon)n_0^{-}(\epsilon)] . \tag{36}$$

Here $n_0^{\pm}(\epsilon)$ is the s density of states in the Wigner-Seitz (WS) sphere. The matrix elements $F_0^{\pm}(\epsilon)$ are given by

$$F_0^{\pm}(\epsilon)=-\frac{4mc}{\hbar}\frac{1}{4\pi}\int_0^{R_{\rm ws}}drR_0^{\pm}(r,\epsilon)\rho_0^{\pm}(r,\epsilon)$$

$$=\frac{1}{4\pi}\int_0^{R_{\rm ws}}dr\frac{\partial S^{\pm}}{\partial r}|R_0^{\pm}(r,\epsilon)|^2 . \tag{37}$$

Due to Eq. (31) in the nonrelativistic limit the matrix elements $F_0^{\pm}(\epsilon)$ approach

$$F_0^{\pm}(\epsilon)\cong\frac{1}{4\pi}|R_0^{\pm}(0,\epsilon)|^2 . \tag{38}$$

IV. LOCAL MOMENTS

In the following we will present the results of extensive calculations for the local moments of the impurities and their nearest neighbors (NN). The aim of this effort was to get an idea of the numerical precision of the calculational procedures as well as of possible systematic errors involved in the exchange correlation approximation.

In order to check for possible numerical errors in the calculation, we have developed a second program for impurity calculations, being in many ways different from the one used by Zeller.[14] For instance Zeller's program is based on a frozen-core approximation and a muffin-tin form of the atomic potentials. Relativistic effects are not included. Moreover only the perturbed charges $\Delta\rho(\mathbf{r})$ inside the cluster of 13 atoms are calculated self-consistently. The exchange-correlation potential used is the one of Moruzzi *et al.*[20] Contrary to that, the present program is based on the embedding philosophy discussed in Sec. II, so that the total charge density $\rho(\mathbf{r})$ is recalculated. Core relaxations are explicitly allowed. Wigner-Seitz potentials are used for the 13 atoms in the cluster and relativistic effects are included in the semirelativistic approximation. Furthermore, three different exchange correlation (XC) potentials are used, i.e., the one of von Barth and Hedin[19] (vBH) or of Vosko, Wilk, and Nusair[21] (VWN) or of Moruzzi, Janak, and Williams[20] (MJW).

Table I shows the calculated moments for $3d$-impurities in Ni. The local moments are defined as the total magnetization within the local Wigner-Seitz sphere. The results for three different XC potentials are given which have been calculated both nonrelativistically (NRL) and semirelativistically (SRA). When we compare the NRL results with the MJW exchange with the ones obtained by Zeller[14] in line 1, we see that both programs yield practically identical results. A noticeable exception is Cr, and to some smaller degree Mn, where appreciable differences occur. We will comment on this problem later on.

The scattering of the moment values for different exchange correlation potentials can give us a feeling for the

TABLE I. Local moments of $3d$ impurities in Ni for different XC potentials in the nonrelativistic (NRL) and scalar relativistic (SRA) approximation. vBH is the von Barth-Hedin XC potential (Ref. 19), MJW is the Moruzzi-Janak-Williams XC potential (Ref. 20), VWN is the Vosko-Wilk-Nusair XC potential (Ref. 21), Z is the theoretical results of Zeller (Ref. 14). The local moments are given in units of μ_B.

		Impurity								
Potential		Sc	Ti	V	Cr	Mn	Fe	Co	Ni	Cu
	Z	−0.14	−0.28	−0.56	−1.69	3.02	2.70	1.70	0.58	−0.01
NRL	vBH	−0.13	−0.25	−0.46	−1.17	2.83	2.63	1.68	0.58	−0.01
	VWN	−0.14	−0.26	−0.50	−1.34	2.91	2.67	1.70	0.59	−0.01
	MJW	−0.14	−0.27	−0.52	−1.40	2.94	2.68	1.71	0.60	−0.01
SRA	vBH	−0.13	−0.25	−0.46	−1.08	2.75	2.62	1.69	0.61	−0.00
	VWN	−0.14	−0.26	−0.50	−1.24	2.84	2.66	1.72	0.62	−0.00
	MJW	−0.14	−0.27	−0.51	−1.31	2.87	2.68	1.73	0.62	−0.00

TABLE II. Local moments of 4d impurities in Ni (same nomenclature as Table I).

Potential		Impurity Y	Zr	Nb	Mo	Tc	Ru	Rh	Pd	Ag
	Z	−0.08	−0.14	−0.21	−0.24	−0.03	0.66	0.57	0.20	−0.01
SRA	vBH		−0.13	−0.18	−0.21	−0.06	0.50	0.54	0.23	−0.00
	VWN		−0.14	−0.20	−0.22	−0.05	0.54	0.56	0.23	−0.00
	MJW	−0.08	−0.14	−0.20	−0.22	−0.05	0.55	0.56	0.24	−0.00

errors involved in the exchange correlation approximation. The results for 3d impurities in Table I and the corresponding results for 4d impurities in Table II show a clear trend. The vBH exchange always gives the smallest moments and the MJW exchange always the largest ones, which the VMN values are intermediate. This behavior has its origin in the polarization dependence of the XC potentials used. One finds that for all densities the exchange splitting of the MJW potential is larger than the vBH one and that the VWN one is intermediate. Therefore the MJW potential shows a somewhat stronger tendency toward magnetism than the VWN one. With the exception of Cr, the absolute magnitude of the differences in Tables I and II is however very small and completely insignificant in comparison with typical experimental errors. We believe therefore that, with the exception of Cr and possibly Mn, the calculated values given in Tables I and II are reliable.

As one expects for 3d impurities, relativistic effects are quite unimportant. For 4d impurities the changes are slightly larger but also rather small so that we have only listed the relativistic results.

Figures 1(a) and 1(b) show the calculated impurity moments for the 3d and 4d impurities in Ni (semirelativistic approximation and VWN exchange). For a detailed comparison with the experimental data we refer to Zeller's paper.[14] Here we want only to comment on why our calculations for Cr yield so widely different results. Whereas Co, Fe, and Mn couple ferromagnetically to the Ni-host moment, Cr, V, Ti, and Sc have an antiparallel moment. Calculations with noninteger nuclear charges Z show[14] that there is a considerable range of Z values for which both a ferromagnetic and antiferromagnetic solution exist, e.g., for Mn. When progressing from Mn to Cr, the ferromagnetic solution becomes instable, whereas when we go from Mn to Fe the antiferromagnetic solution disappears. Thus both for Cr and Mn one is close to instabilities and any small change in the numerical procedures or in the XC potential can lead to large differences. Physically this is due to the fact that at the instability the susceptibilities of the system diverge. This is a severe problem for Cr, where the calculated values range from -1.08 to $-1.70\mu_B$. The uncertainty is sufficiently large that we should not take the disagreement with the experimental value of $-0.2\pm0.6\mu_B$ (Ref. 37) serious. For Mn this problem also exists, however here the uncertainty is considerably smaller. However in the other cases we consider our calculations as reliable. Especially we believe that the very large moment of about $2\mu_B$ reported for Rh in Ni (Ref. 38) is unrealistic.

The changes of the moment on a neighboring host atom are listed in Table III. The moment is only slightly changed when the impurity moment aligns to the host moments, but strongly decreases for the antiparallel con-

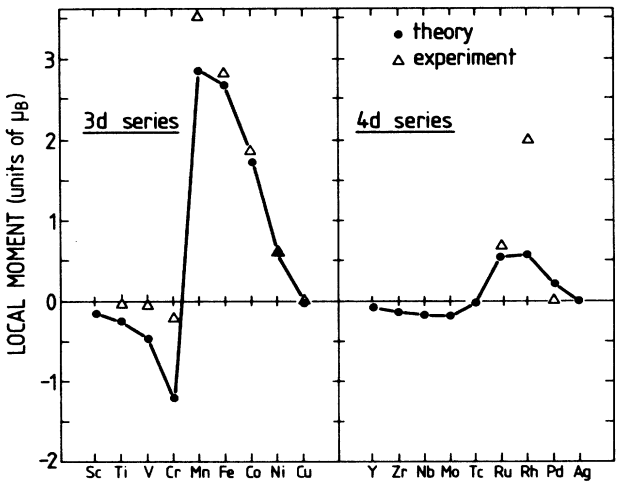

FIG. 1. Calculated local moments for 3d impurities and 4d impurities in Ni. The calculations refer to the semirelativistic approximation with VWN exchange correlation. The triangles denote experimental values.

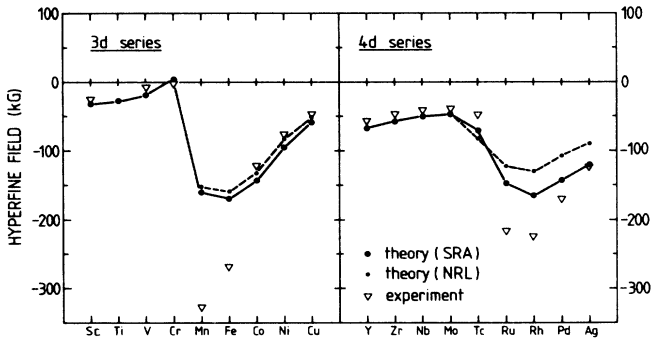

FIG. 2. Calculated hyperfine fields for 3d and 4d impurities in Ni. The large dots refer to the semirelativistic approximation the small ones to the nonrelativistic calculation. The experimental values (▽) are taken from a recent data collection (Ref. 2).

TABLE III. Change of the moment of a nearest-neighbor Ni atom (same nomenclature as Table I).

Potential		Impurity Sc	Ti	V	Cr	Mn	Fe	Co	Ni	Cu
SRA	vBH	−0.15	−0.19	−0.20	−0.19	−0.03	−0.01	+0.01	0.00	−0.03
	VWN	−0.15	−0.19	−0.20	−0.19	−0.03	−0.01	+0.00	0.00	−0.03
	MJW	−0.15	−0.19	−0.20	−0.19	−0.03	−0.01	+0.00	0.00	−0.03

Potential		Impurity Y	Zr	Nb	Mo	Tc	Ru	Rh	Pd	Ag
SRA	VWN	−0.18	−0.22	−0.25	−0.27	−0.23	−0.07	−0.01	−0.01	−0.04

figuration.[14] Table III demonstrates that these changes are very insensitive to the form of the XC potential.

V. HYPERFINE FIELDS

Table IV gives the calculated hyperfine fields of $3d$ impurities in Ni, Table V gives the corresponding values for the $4d$ impurities. Listed are both the nonrelativistic (NRL) and the relativistic results (SRA). The values refer to the VWN exchange correlation potential. Figures 2(a) and 2(b) show a comparison between the calculated and experimental data. We obtain strong negative values for the ferromagnetically aligned impurities (Co, Fe, Mn and Pd, Rh, Ru) and moderately negative ones for the impurities with negative moments (Cr, . . . , Sc and Tc, . . . , Y). For both series the values for the antiferromagnetic impurities agree very well with the experiments, however there are serious disagreements for the ferromagnetically aligned impurities. Especially the calculated values for Fe and Mn, the impurities with the largest moments, are far too small. In the $4d$ series the values for Rh and Ru are also somewhat too small. We will come back to these discrepancies later. Despite these deficiencies we can say that our calculations reproduce the experimentally observed trends of the hyperfine fields.

Tables IV and V as well as Fig. 2 contain both the relativistic as well as the nonrelativistic results. In general we see that in the $3d$ series the relativistic corrections are rather small, typically 10% for the ferromagnetic impurities. Contrary for the $4d$ series, the corrections are quite important. For Rh, Pd, and Ag they are as large as 30% and lead to a considerable improvement of the nonrelativistic values. Note that the valence properties, especially the local moments, are changed only very little due to relativistic effects. The comparatively large corrections for the hyperfine fields arise mostly from the inner core region where the Coulomb potential is large so that relativistic effects become important. The corrections are however considerably smaller than the relativistic enhancement of the charge densities at the origin. For instance for Fe, we have a nearly 50% enhancement of the charge and spin density near the origin. Thus the relativistic correction for the hyperfine fields would be grossly in error, if the Fermi contact interaction formula, instead of the correct Breit formula, were used. Our calculated corrections are in reasonable agreement with the values given by Pyykkö *et al.*[33] for hydrogenlike models. For instance for the neighboring Ni atoms the enhancement is around 9—10% for all impurities studied in agreement with Pyykkö *et al.* However, sizable deviations can occur if the valence properties, especially the local moments, are changed by relativistic corrections. Then the enhancement can be considerably larger or smaller than the hydrogenic values. For example, for V we obtain an enhancement of 23%, compared to 6% of Pyykkö *et al.*; for Mo the enhancement is 34% instead of 23% for the hydrogenic model. Thus the hydrogenlike corrections given by Pyykkö *et al.* are of limited usefulness.

Table VI shows the dependence of the hyperfine fields on the exchange correlation potentials. Similar to the re-

TABLE IV. Hyperfine fields of $3d$ impurities in Ni. Listed are the calculated hyperfine fields in the nonrelativistic (NRL) and semirelativistic approximation using the VWN XC potential. $H_{\rm hf}^{c}$ is the core contribution, $H_{\rm hf}^{v}$ the valence one, and $H_{\rm hf}^{t}=H_{\rm hf}^{c}+H_{\rm hf}^{v}$ the total value. The experimental values $H_{\rm hf}^{\rm expt}$ are taken from Krane (Ref. 2). All data in kG.

Hyperfine fields		Impurity Sc	Ti	V	Cr	Mn	Fe	Co	Ni	Cu
NRL	$H_{\rm hf}^{c}$	13	24	45	122	−277	−261	−172	−64	−3
	$H_{\rm hf}^{v}$	−41	−47	−61	−111	124	103	40	−20	−48
	$H_{\rm hf}^{t}$	−28	−23	−16	11	−152	−158	−132	−84	−51
SRA	$H_{\rm hf}^{c}$	13	25	47	121	−292	−283	−191	−74	−4
	$H_{\rm hf}^{v}$	−44	−52	−67	−116	131	114	48	−21	−55
	$H_{\rm h}^{t}$	−31	−27	−19	5	−160	−169	−143	−95	−59
	$H_{\rm hf}^{\rm expt}$	−26		−7	−3	−328	−270	−121	−76	−47

TABLE V. Hyperfine fields of 4d impurities in Ni (same nomenclature as in Table IV).

Hyperfine fields		Impurity Y	Zr	Nb	Mo	Tc	Ru	Rh	Pd	Ag
NRL	H_{hf}^{c}	17	27	36	37	1	−100	−89	−34	−2
	H_{hf}^{v}	−71	−73	−74	−73	−58	−23	−41	−73	−88
	H_{hf}^{t}	−55	−46	−38	−36	−58	−123	−130	−107	−90
SRA	H_{hf}^{c}	19	33	44	47	7	−123	−126	−57	−7
	H_{hf}^{v}	−88	−90	−94	−95	−78	−24	−39	−85	−113
	H_{hf}^{t}	−68	−57	−50	−48	−71	−147	−165	−142	−120
	H_{hf}^{expt}	−57	−47	−41	−40	−48	−217	−225	−170	−122

sults for the moments (Tables I and II) the vBH potential gives normally the smallest and the MJW potential the largest value for the hyperfine fields of the impurities. The differences are typically 10% and considerably larger than the corresponding difference for the local moments.

Next we discuss the individual contributions to the hyperfine fields, i.e., the core and valence contributions which are listed in Tables IV and V. The *core polarization* is large for magnetic impurities. It is due to the exchange interaction of the polarized d shell with the s orbitals of the core. As a result a weak s polarization is induced at the nuclear position, which is in general opposite to the local moment. Since the exchange interaction is weak the core polarization and thus the core hyperfine field H_{hf}^{c} is expected to scale with the local moment M_{loc}. Figures 3 and 4 illustrate that this is indeed the case. Plotted are the local moments (left scale) and the core hyperfine fields (inverted right scale) for both the 3d and 4d series. Since the curves for the local moments and the core hyperfine fields more or less coincide we obtain the following simple relation: $H_{hf}^{c}=CM_{loc}$ with $C\cong -100$ kG/μ_B for the 3d series and $C\cong -200$ kG/μ_B for the 4d series. That the core polarization is opposite to the local moment, i.e., $C<0$, has been explained by Freeman and Watson[39] and can qualitatively be understood as follows. The majority s electrons in the core will be pulled into the region of the spin-polarized d shell, since the exchange interaction is attractive, whereas the minority electrons will be repelled from the d shell. At the nuclear position we have therefore an excess of minority electrons, i.e., a negative polarization. A closer look at the data in the Tables I, II, IV, and V reveals that the constant C slowly changes in the 3d and 4d series. For instance in the 3d series the lowest value is −95 for Ti and V, the highest one is −120 for Ni, whereas in the 4d series the constant C varies from −203 for Y to −243 for Pd. This variation is due to the change of the valence-d and core-s wave functions through the transition metal series and therefore not surprising at all. On the contrary it is surprising that the variation is so small.

Despite the fact that the total core polarization is always opposite in sign to the local moment, the individual contributions from the 1s, 2s, ... shells can have different signs. Table VII shows the shell decomposition of the hyperfine fields for the 3d elements, V and Fe, and the 4d ones, Nb and Ru. Note that V and Nb have a negative

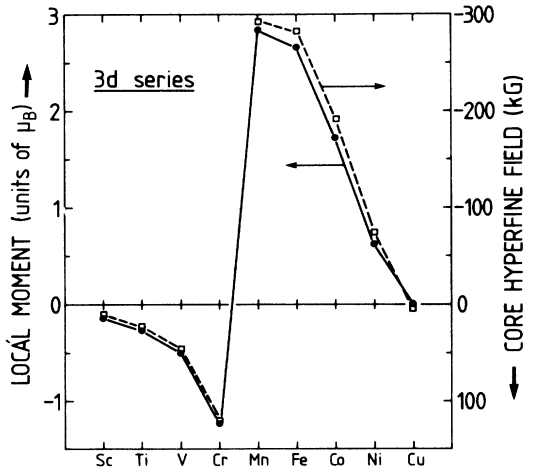

FIG. 3. Core hyperfine fields (right scale) and local moments (left scale) for 3d impurities in Ni. Note the inverted scale for the core hyperfine fields.

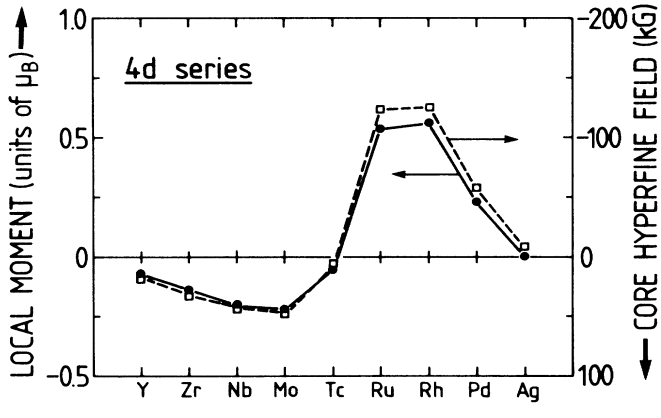

FIG. 4. Core hyperfine fields (right scale) and local moments (left scale) for 4d impurities in Ni. Note the inverted scale for the core hyperfine fields.

TABLE VI. Hyperfine fields for $3d$ and $4d$ impurities in Ni. The table gives the hyperfine field values, calculated in the semirelativistic approximation for three different exchange-correlation potentials. All data in kG.

Potentials	Impurity Sc	Ti	V	Cr	Mn	Fe	Co	Ni	Cu
vBH	−29	−25	−18	1	−150	−160	−136	−90	−56
VWN	−28	−28	−16	11	−152	−158	−132	−84	−51
MJW	−31	−27	−20	6	−163	−171	−146	−97	−61
Potentials	Impurity Y	Zr	Nb	Mo	Tc	Ru	Rh	Pd	Ag
vBH		−53	−46	−44	−64	−135	−154	−133	−112
VWN		−57	−50	−48	−71	−147	−165	−142	−120
MJW	−68	−58	−51	−49	−72	−151	−168	−144	−122

moment, whereas the moment of Fe and Ru is positive (with respect to the host moment). In the $3d$ series the $1s$ and especially the $2s$ contribution are opposite to the local moment, whereas the $3s$ contribution has the same sign as the local moment. In the $4d$ series the most important contributions come from the $2s$ and $4s$ levels. Both are opposite to the local moments.

The *valence contributions* to the hyperfine fields are more complicated. They are plotted in Figs. 5 and 6 for the $3d$ and $4d$ impurities (right scale) together with the corresponding local moments (left scale). It is seen that up to a more or less constant negative contribution the valence hyperfine fields follow closely the local moment curves. The constant negative contribution is quite analogous to the negative hyperfine field of the early *sp* impurities.[4–6,9] The hybridization of the impurity *s* orbitals with the spin-polarized *d* orbitals of the neighboring Ni atoms induces a weak *s* polarization, which is negative for the early *sp* impurities. This *"transferred hyperfine field"* is also negative for the transition metal impurities, since their potentials are weak in the sense of Katayama *et al.*[4–6] One expects the transferred contribution to be essentially proportional to the local moments of the neighboring host atoms. Since these moments are strongly reduced for the impurities with negative moments (Sc, ..., Cr and Y, ..., Tc) the corresponding transferred fields should be substantially smaller than the ones of the ferromagnetic impurities. Indeed Figs. 5 and 6 give an indication of such an effect, since the difference between the local moment curve and the valence field curve is substantially reduced for the impurities with negative moments.

In addition to this negative transferred hyperfine field we obtain for magnetic impurities a *"local valence hyperfine field"* which dominates the behavior seen in Figs. 5 and 6. The figures demonstrate that this local contribution is proportional to the local moment; however contrary to the core hyperfine field the proportionality constant is positive. It is tempting to interpret this behavior analogous to the core polarization, i.e., the *s-d* exchange interaction pulls the majority valence *s* electrons inward and pushes the minority *s* electrons outward so that the polarization at the nucleus is positive. However this ef-

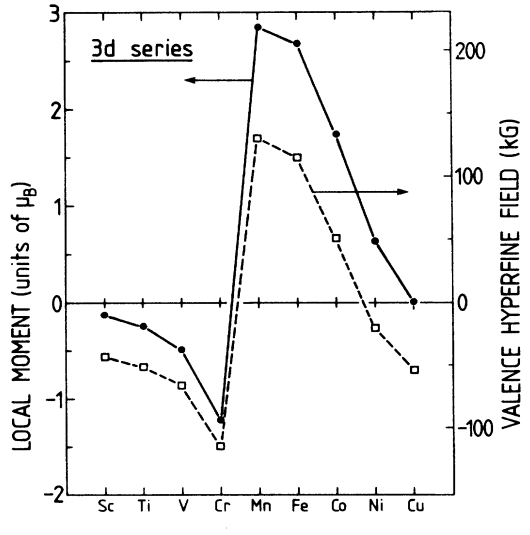

FIG. 5. Valence hyperfine fields (right scale) and local moments (left scale) for $3d$ impurities in Ni.

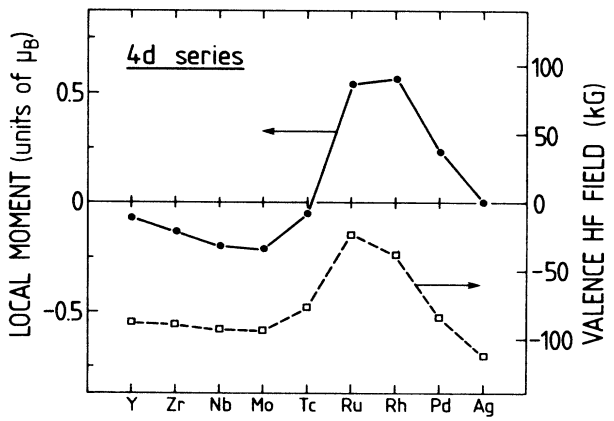

FIG. 6. Valence hyperfine fields (right scale) and local moments (left scale) for $4d$ impurities in Ni.

TABLE VII. Shell decomposition of the hyperfine fields. Decomposition of the hyperfine field of V, Fe, Nb, and Ru into the different shell contributions (semirelativistic approximation with VWN XC potentials).

	1s	2s	3s	4s	Total	
V	2	65	−20	−67	−19	
Fe	−23	−603	342	114	−169	
	1s	2s	3s	4s	5s	Total
Nb	1	8	−2	36	−94	−50
Ru	−5	−46	3	−75	−24	−147

fect is of minor importance for the valence electrons. The dominating mechanism is a repopulation effect, i.e., more majority and less minority s states are occupied, leading to a valence s moment in the impurity Wigner-Seitz cell. Figure 7 shows, that the valence hyperfine field is in a rather good approximation proportional to this local s moment. A similar proportionality is also obtained within the $4d$ series. Going back to Eq. (36) we conclude that for the valence hyperfine fields the difference between the spin-up and spin-down density of states is most important. The matrix elements $F^{\pm}(\epsilon)\cong(1/4\pi)\,|\,R_s^{\pm}(0,\epsilon)\,|^2$ do not depend strongly on the spin direction nor on the energy, so that in a rough approximation ΔE is proportional to the local s moment M_s:

$$M_s=\int^{\epsilon_F} d\epsilon[n_s^{+}(\epsilon)-n_s^{-}(\epsilon)]\ .$$

The proportionality constant, essentially given by a suitable average of the square of the s-wave function at the origin, is more or less the same throughout the whole $3d$ series.

We will now discuss the *hyperfine fields of the neighboring Ni atoms,* which are listed in Table VIII. Figure 8 shows the change of the hyperfine field (left scale) of a NN Ni atom with respect to a bulk Ni atom together with the change of the corresponding local Ni moment (right inverted scale). Both for the moments and for the hyperfine fields we obtain similar s-shaped curves. According to the above discussion this strongly indicates that the local contributions (of core and valence) to $\Delta H_{\rm hf}$ are important. However there are also indications for important transferred contributions. For instance for Co, Fe, and Mn the local moments on the neighboring sites are practically unchanged. Here the negative values for $\Delta H_{\rm hf}$ arise from the large impurity moments on the adjacent site leading to a negative transferred hyperfine contribution proportional to the change $\Delta M=M_{\rm imp}-M_{\rm Ni}$ of the moment on the impurity site. Contrarily for Cr, V, and Ti as well as for Mo, Nb, ..., the change ΔM is negative, resulting in a sizable transferred contribution to ΔH which is positive.

The division of the hyperfine field into a local and a transferred contribution and the above discussion suggest a simple *interpolation formula* for the hyperfine fields in terms of the moments of the considered atom and its neighbors. We therefore set

$$H_{\rm hf}=aM_{\rm loc}+bM_{\rm host}+c\sum_{i=\rm NN}\Delta M_i\ .$$

The first term $aM_{\rm loc}$ represents the local hyperfine field, being the sum of the local core and valence contributions, which are both proportional to the local moment (see Fig. 1). From the behavior of the hyperfine field through the $3d$ and $4d$ series (Fig. 2) it is clear that the constant a is negative since the core contribution dominates. The second and third terms represent the

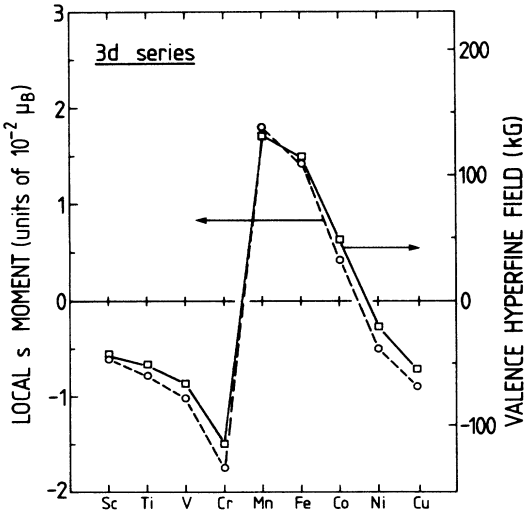

FIG. 7. Valence hyperfine fields (right scale) and local s moments (left scale) for $3d$ impurities in Ni.

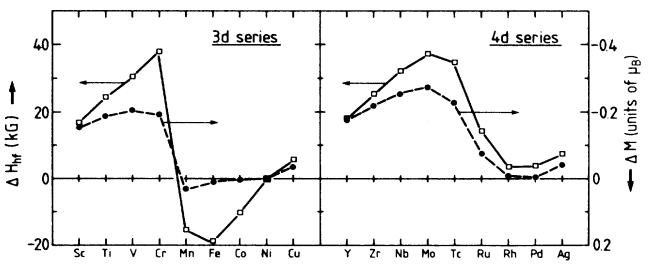

FIG. 8. Change of the hyperfine field of a nearest-neighbor (NN) atom (left scale) and change of the NN Ni moment (right inverted scale) for $3d$ and $4d$ impurities in Ni.

TABLE VIII. Change of the hyperfine fields of NN Ni atoms. The change of the hyperfine field $\Delta H^t_{\rm hf}$ of NN Ni atoms with respect to a bulk Ni atom is given. $\Delta H^c_{\rm hf}$ and $\Delta H^v_{\rm hf}$ denote the core and valence contributions.

	Sc	Ti	V	Cr	Mn	Fe	Co	Ni	Cu
$\Delta H^c_{\rm hf}$	18	22	24	23	4	1	−1	0	4
$\Delta H^v_{\rm hf}$	−1	2	6	15	−20	−20	−9	0	2
$\Delta H^t_{\rm hf}$	17	24	30	38	−16	−19	−10	0	6
	Y	Zr	Nb	Mo	Tc	Ru	Rh	Pd	Ag
$\Delta H^c_{\rm hf}$	20	25	30	32	27	9	1	1	5
$\Delta H^v_{\rm hf}$	−2	0	3	5	8	5	2	3	2
$\Delta H^t_{\rm hf}$	18	25	32	37	34	14	3	4	7

transferred hyperfine field consisting of a constant contribution $bM_{\rm host}$ and a correction $c\sum_i \Delta M_i$ if the moments M_i on the neighboring sites are changed by the amount ΔM_i. Further ranging changes are neglected. Clearly the constants b and c are negative, since the potentials of the transition metals are weak in the sense of Katayama *et al.*[4–6] An ansatz similar to the above one has already been made by Campbell[40] in trying to analyze the experimental data for Fe. By taking the calculated values for the moments of the impurities and the nearest neighbors (Tables I, II, and III) the constants a, b, and c can be determined by fitting the above ansatz to the calculated hyperfine fields of the $3d$ impurities (Table IV) and their nearest neighbors (Table V). A reasonable fit of both sets of hyperfine fields is obtained with

$$a \cong -37,\quad b \cong -115,\quad c \cong -10.4 \text{ (in units of kG}/\mu_B\text{)}.$$

For the $4d$ series, a reasonable fit of the calculated impurity hyperfine fields is obtained with

$$a \cong -88,\quad b \cong -199,\quad c \cong -15.4 \text{ (in units of kG}/\mu_B\text{)}.$$

It is clear that such a fit cannot accurately reproduce the calculated values. For instance we have discussed that the core hyperfine field is not accurately proportional to the local moment. Similar arguments apply also for the valence hyperfine field. Nevertheless we believe that the important trends of the calculated hyperfine fields for $3d$ and $4d$ impurities are well represented by the above relation.

We will now discuss the *limitations of our calculations*. From Fig. 2 it is clear that while our calculations reproduce the experimentally observed trends of the hyperfine fields there are serious differences in cases where the local moment is large. This includes Fe and Mn impurities in Ni, but also, e.g., pure Fe. What are the reasons for these failures?

In our calculations we have completely neglected lattice relaxations of the neighboring atoms. However at least for neighboring atoms such as Co in Ni or Fe in Ni, relaxations are rather small. They are expected to be somewhat bigger for the early $3d$ impurities and for $4d$ impurities. In general, however, the effect on the local moments and the hyperfine fields are not expected to be so large that the discrepancies for Fe and Mn could be explained.

Our calculations are semirelativistic, i.e., we take mass-velocity and Darwin-like terms into account while neglecting spin-orbit coupling. We obtain, therefore, no orbital contribution to the hyperfine field. Independently of the magnitude of such a contribution, its sign should be positive for Fe and Mn. Therefore, if anything, it would enhance the discrepancies between theory and experiment. Dipolar contributions vanish for the impurities due to the cubic point symmetry. We have estimated them for the change of the hyperfine fields of the neighboring atoms and obtain small corrections of 1–2 % of the values given in Table VIII.

Another source of error could be relativistic corrections to the local exchange potential as have been discussed by Ramana and Rajagopal.[41] Due to the rather high core densities such effects could be important for the hyperfine fields. Since the exchange-correlation potential is still local, their inclusion does not complicate the calculations. Weinert and Freeman[42] have recently included such relativistic corrections for the paramagnetic exchange potential in Knight-shift calculations for Pt surfaces. Here the corrections are quite small and negligible. However it remains to be seen if this is also true for the spin-dependent exchange potential as derived in Ref. 41.

Presumably the most serious approximation in our calculation is the local density approximation. While it is now well established that local moments can be calculated quite successfully within this approximation, the application to hyperfine fields is a different matter. While the results for nonmagnetic impurities[4–6,9] seem to indicate that the transferred part of the hyperfine field can be calculated reasonably well, the present results for magnetic impurities, especially for Fe and Mn impurities, indicate serious errors for the local contribution to the hyperfine field. Since the latter contribution arises from the inherently nonlocal s-d exchange interaction deep in the core, it seems to be natural to assume that the local density approximation is the reason for this failure. This is in line with the argument of Wilk and Vosko based on atomic calculations.[8] Nevertheless the errors are not as big as one would expect from the latter publication, since the general trends for the $3d$ and $4d$ impurities are well represented.

VI. SUMMARY

We have performed detailed self-consistent calculations for the hyperfine fields of transition-metal impurities in Ni. New formulas for the relativistic generalizations of the contact, orbital, and dipolar contributions to the hyperfine fields are derived. For the relativistic contact interaction the spin-density near the nucleus has to be averaged over a region whose diameter is the Thomson radius.

For transition metal impurities the core polarization induced by *sd* exchange leads to a large core hyperfine field being negative and proportional to the local moment. In addition an important valence hyperfine field is obtained consisting of a transferred and a local contribution. The transferred field is negative for transition-metal impurities and arises from the hybridization with the spin-polarized *d* electrons of the Ni neighbors, as explained by Katayama *et al.*[4–6] The local valence field is directly proportional to the local moment, but contrary to the core field it is positive. It is caused by the enhanced population of the majority *s*-states.

The calculations reproduce the experimentally observed trends for the hyperfine fields. However for large moment cases appreciable discrepancies occur which we believe are due to failures of the local density approximation in describing the core polarization.

---

*Permanent address: Nara Medical University, Kashihara, Nara 634, Japan.

[1]G. N. Rao, Hyperfine Interact. **7**, 141 (1979).
[2]K. S. Krane, Hyperfine Interact. **16**, 1069 (1983).
[3]E. Daniel and J. Friedel, J. Phys. Chem. Solids **24**, 1601 (1963).
[4]H. Katayama, K. Terakura, and J. Kanamori, Solid State Commun. **29**, 431 (1979).
[5]H. Katayama-Yoshida, K. Terakura, and J. Kanamori, J. Phys. Soc. Jpn. **46**, 822 (1979); **48**, 1504 (1980); **49**, 972 (1980).
[6]J. Kanamori, H. Katayama-Yoshida, and K. Terakura, Hyperfine Interact. **8**, 573 (1981).
[7]J. F. Janak, Phys. Rev. B **20**, 2206 (1979).
[8]L. Wilk and S. H. Vosko, Phys. Rev. A **15**, 1839 (1977).
[9]M. Akai, H. Akai, and J. Kanamori, J. Phys. Soc. Jpn. **54**, 4246 (1985).
[10]H. Akai, M. Akai, and J. Kanamori, J. Phys. Soc. Jpn. **54**, 4257 (1985).
[11]See, e.g., R. Podloucky, R. Zeller, and P. H. Dederichs, Phys. Rev. B **22**, 5777 (1980).
[12]P. Leonard and N. Stefanou, Philos. Mag. B **51**, 151 (1985).
[13]R. Zeller, in *Physics of Transition Metals, 1980,* IOP Conf. Ser. No. 55, edited by P. Rhodes (IOP, London, 1981), p. 265.
[14]R. Zeller (unpublished).
[15]S. Blügel, Diplomarbeit, Technische Hochschule, Aachen, 1983.
[16]G. Breit, Phys. Rev. **35**, 1447 (1930).
[17]P. H. Dederichs, R. Zeller, H. Akai, S. Blügel, and A. Oswald, Philos. Mag. B **51**, 137 (1985).
[18]H. Akai, M. Akai, S. Blügel, R. Zeller, and P. H. Dederichs, J. Magn. Magn. Mater. **45**, 291 (1984).
[19]U. von Barth and L. Hedin, J. Phys. C **5**, 1629 (1972).
[20]V. L. Moruzzi, J. F. Janak, and A. R. Williams, *Calculated Electronic Properties of Metals* (Pergamon, New York, 1978).
[21]S. H. Vosko, L. Wilk, and M. Nusair, J. Can. Phys. **58**, 1200 (1980).
[22]D. M. Ceperley and B. J. Alder, Phys. Rev. Lett. **45**, 566 (1980).
[23]P. J. Braspenning, R. Zeller, A. Lodder, and P. H. Dederichs, Phys. Rev. B **29**, 703 (1984).
[24]O. Gunnarsson, O. Jepsen, and O. K. Andersen, Phys. Rev. B **27**, 7144 (1983).
[25]H. Akai, S. Blügel, R. Zeller, and P. H. Dederichs, Phys. Rev. Lett. **56**, 2407 (1986).
[26]See, e.g., F. Rosicky, P. Weinberger, and F. Mark, J. Phys. B **9**, 2971 (1976).
[27]See, e.g., E. M. Rose, *Relativistic Electron Theory* (Wiley, New York, 1961).
[28]D. D. Koelling and B. N. Harmon, J. Phys. C **10**, 3107 (1977).
[29]T. Takeda, Z. Phys. B **32**, 43 (1978).
[30]E. Fermi, Z. Phys. **60**, 320 (1930).
[31]E. Wimmer, A. J. Freeman, and H. Krakauer, Phys. Rev. B **30**, 3113 (1984).
[32]T. Asada and K. Terakura, J. Phys. F **12**, 387 (1982).
[33]P. Pyykkö, E. Pajanne, and M. Inokuti, Int. J. Quantum Chem. **7**, 785 (1973).
[34]T. Asada and K. Terakura, J. Phys. F **13**, 799 (1983).
[35]*Mössbauer Isomer Shifts,* edited by G. E. Shenoy and F. E. Wegner (North-Holland, Amsterdam, 1978).
[36]D. A. Shirley, Rev. Mod. Phys. **36**, 339 (1964).
[37]J. W. Cable and R. A. Medina, Phys. Rev. B **13**, 4868 (1976).
[38]J. W. Cable, Phys. Rev. **15**, 3477 (1977).
[39]A. J. Freeman and R. E. Watson, in *Magnetism,* edited by G. T. Rado and H. Suhl (Academic, New York, 1965), Vol. II A.
[40]I. A. Campbell, Proc. Phys. Soc. **89**, 71 (1966).
[41]M. V. Ramana and A. K. Rajagopal, J. Phys. C **14**, 4291 (1981).
[42]M. Weinert and A. J. Freeman, Phys. Rev. B **28**, 6262 (1983).